

PATH INTEGRAL MONTE CARLO APPROACH TO THE U(1) LATTICE GAUGE THEORY IN (2+1) DIMENSIONS

Mushtaq Loan*, Michael Brunner, Clare Sloggett and Chris Hamer

School of Physics, University of New South Wales, Sydney, Australia

(September 24, 2002)

Abstract

Path Integral Monte Carlo simulations have been performed for U(1) lattice gauge theory in (2+1) dimensions on anisotropic lattices. We extract the static quark potential, the string tension and the low-lying “glueball” spectrum. The Euclidean string tension and mass gap decrease exponentially at weak coupling in excellent agreement with the predictions of Polyakov and Göpfert and Mack, but their magnitudes are five times bigger than predicted. Extrapolations are made to the extreme anisotropic or Hamiltonian limit, and comparisons are made with previous estimates obtained in the Hamiltonian formulation.

Typeset using REVTEX

*e-mail :mushe@newt.phys.unsw.edu.au

I. INTRODUCTION

Classical Monte Carlo simulations [1] of the path integral in Euclidean lattice gauge theory [2] have been very successful, and this is currently the preferred method for *ab initio* calculations in quantum chromodynamics (QCD) in the low energy regime. Monte Carlo approaches to the Hamiltonian version of QCD propounded by Kogut and Susskind [3] have been less successful, however, and lag at least ten years behind the Euclidean calculations. Our aim in this paper is to see whether useful results can be obtained for the Hamiltonian version by using the standard Euclidean Monte Carlo methods for anisotropic lattices [4], and extrapolating to the Hamiltonian limit in which the time variable becomes continuous, i.e. the lattice spacing in the time direction goes to zero. The Hamiltonian version of lattice gauge theory is less popular than the Euclidean version, but is still worthy of study. It can provide a valuable check of the universality of the Euclidean results [5], and it allows the application of many techniques imported from quantum many-body theory and condensed matter physics, such as strong coupling expansions [6], the t-expansion [7], the coupled-cluster method [8] and more recently the density matrix renormalization group [9] (DMRG). None of these techniques has proved as useful as Monte Carlo in (3+1) dimensions; but in lower dimensions they are more competitive.

A number of Quantum Monte Carlo methods have been applied to Hamiltonian lattice gauge theory in the past, with somewhat mixed results. A “Projector Monte Carlo” approach [10,11] using a strong coupling representation for the gauge fields runs into difficulties for non-Abelian models, in that it requires Clebsch-Gordan coefficients for SU(3) which are not even known at high orders; and furthermore a version of the “minus sign problem” rears its head [12]. A Greens Function Monte Carlo approach was pioneered by Chin et al [13] and Heys and Stump [14], which uses a weak coupling representation for the gauge fields. This approach can be used successfully for non-Abelian theories, and obtains estimates of parameters such as the string tension and glueball masses from the correlation functions in a similar fashion to Euclidean techniques. Unfortunately the approach requires the use of a “trial wave function” to guide random walkers in the ensemble towards the preferred regions of configuration space [15]. This introduces a variational element into the procedure, in that the results may exhibit a systematic dependence on the trial wave function. We have previously explored [16,19,20] a “forward-walking” technique [21,22] for measuring the expectation values and the correlation functions, which should minimize this dependence; but calculations for the SU(3) Yang-Mills theory in (3+1) dimensions still showed an unacceptably strong sensitivity to the parameters of the trial wave function [20]. For this reason, we are forced to look yet again for an alternative approach.

As mentioned above our aim in this paper is to use standard Euclidean path integral Monte Carlo techniques for anisotropic lattices, and see whether useful results can be obtained in the Hamiltonian limit. Morningstar and Peardon [4] showed some time ago that the use of anisotropic lattices can be advantageous in any case, particularly for the measurement of glueball masses. We use a number of their techniques in what follows.

As a first trial of this approach, we treat the U(1) gauge model in (2+1)D, which is one of the simplest models with dynamical gauge degrees of freedom, and has also been studied extensively by other means (see Section II). Path integral Monte Carlo methods were applied to this model a long time ago by Hey and collaborators [23,24], but the techniques used at

that time were not very sophisticated, and the results were rather qualitative. Very little has been done since then using this approach on this particular model.

The rest of this paper is organised as follows. In section II we discuss the U(1) model in (2+1) dimensions in its lattice formulation, and outline some of the work done on it previously. The details of the simulations, including the generation of the gauge-field configurations, the construction of the Wilson loop operators and glueball operators, and the extraction of the potential and string tension estimates are described in section III. In section IV we present our main results for the mean plaquette, static quark potential, string tension and glueball masses. The static quark potential has not previously been exhibited for this model, as far as we are aware. Finally we make an extrapolation to the Hamiltonian limit, and comparisons are made with estimates obtained by other means in that limit. We find that indeed the PIMC method can give better results than other weak-coupling Monte Carlo methods, even in the Hamiltonian limit. Our conclusions are summarized in Sec. VI.

II. THE U(1) MODEL

Consider the isotropic Abelian U(1) lattice gauge theory in three dimensions. The theory is defined by the action [2]

$$S = \beta \sum_{r,\mu,\nu} \text{ReTr} P_{\mu\nu} \quad (1)$$

where

$$P_{\mu\nu}(r) = [1 - \text{ReTr}\{U_\mu(r)U_\nu(r + \hat{\mu})U_\mu^\dagger(r + \hat{\nu})U_\nu^\dagger(r)\}] \quad (2)$$

is the plaquette variable given by the product of the link variables taken around an elementary plaquette. The link variable $U_\mu(r)$ is defined by

$$U_\mu(r) = \exp[ieaA_\mu(r)] = \exp[i\theta_\mu(r)] \quad (3)$$

where in the compact form of the model, $\theta_\mu(r)(= eaA_\mu(r)) \in [0, 2\pi]$ represents the gauge field on the directed link $r \rightarrow r + \hat{\mu}$. The parameter β is related to the bare gauge coupling by

$$\beta = \frac{1}{g^2} \quad (4)$$

where $g^2 = ae^2$, in (2+1) dimensions.

The lattice U(1) model in (2+1) dimensions has been studied by many authors, and possesses some important similarities with QCD (for a more extensive review, see for example ref. [12]). If one takes the “naive” continuum limit at a fixed energy scale, one regains the simple continuum theory of non-interacting photons [25]; but if one renormalizes or rescales in the standard way so as to maintain the mass gap constant, then one obtains a confining theory of free massive bosons. Polyakov [26] showed that a linear potential appears between static charges due to instantons in the lattice theory; and Göpfert and Mack [27] proved that in the continuum limit the theory converges to a scalar free field theory of massive bosons. They found that in that limit the mass gap behaves as

$$am_D = \sqrt{\frac{8\pi^2}{g^2}} \exp\left(-\frac{\pi^2}{g^2}v(0)\right) \quad (5)$$

while the string tension is bounded by

$$a^2\sigma \geq c\sqrt{\frac{g^2}{2\pi^2}} \exp\left(-\frac{\pi^2}{g^2}v(0)\right) \quad (6)$$

where $v(0)$ is the Coulomb potential at zero distance, and has a value in lattice units

$$v(0) = 0.2527 \quad (7)$$

for the isotropic case. They argue that (6) represents the true asymptotic behaviour of the string tension, where the constant c is equal to 8 in classical approximation. The theory has a non-vanishing string tension for arbitrarily large β , similar to the behaviour expected for non-Abelian lattice gauge theories in four dimensions.

For an anisotropic lattice, the gauge action becomes [4]

$$S = \beta_s \sum_{r,i < j} P_{ij}(r) + \beta_t \sum_{r,i} P_{it}(r) \quad (8)$$

where P_{ij} and P_{it} are the spatial and temporal plaquette variables respectively. In the classical limit

$$\beta_s = \frac{a_t}{e^2 a_s^2} = \frac{1}{g^2} \Delta\tau \quad (9)$$

$$\beta_t = \frac{1}{e^2 a_t} = \frac{1}{g^2} \frac{1}{\Delta\tau} \quad (10)$$

where $\Delta\tau = a_t/a_s$ is the anisotropy parameter, a_s is the lattice spacing in the space direction, and a_t is the temporal spacing. The above action can be written as

$$S = \beta \left[\Delta\tau \sum_r \sum_{i < j} \left(1 - \cos \theta_{ij}(r) \right) + \frac{1}{\Delta\tau} \sum_{r,i} \left(1 - \cos \theta_{it}(r) \right) \right] \quad (11)$$

In the limit $\Delta\tau \rightarrow 0$, the time variable becomes continuous, and we obtain the Hamiltonian limit of the model (modulo a Wick rotation back to Minkowski space).

The behaviour of the mass gap in the anisotropic case will be similar to equation (5). Generalizing discussions by Banks *et al* [28] and Ben-Menahem [29], we find that the exponential factor takes exactly the same form in the anisotropic case. The only difference is that the lattice Coulomb potential at zero spacing for general $\Delta\tau$ is

$$v(0) = \int_{-\pi}^{\pi} \frac{d^3k}{(2\pi)^3} \frac{\Delta\tau}{4[\sin^2(k_0/2) + \Delta\tau^2(\sin^2(k_1/2) + \sin^2(k_2/2))]} \quad (12)$$

$$= \begin{cases} 0.2527 & (\Delta\tau = 1) \\ 0.3214 & (\Delta\tau = 0) \end{cases} \quad (13)$$

But this result neglects the effects of monopoles with charges other than 0, ± 1 in the monopole gas, which is justified in the Euclidean case, but not in the Hamiltonian limit [28,29].

The Hamiltonian version of the model has been studied by many methods: some recent studies include series expansions [30], finite-lattice techniques [32], the t-expansion [33,34], and coupled-cluster techniques [35–37], as well as Quantum Monte Carlo methods [13,38,39,12,18,17,19]. Quite accurate estimates have been obtained for the string tension and the mass gaps, which can be used as comparison for our present results. The finite-size scaling properties of the model can be predicted using an effective Lagrangian approach combined with a weak-coupling expansion [40], and the predictions agree very well with finite-lattice data [12].

III. METHODS

A. Path Integral Monte Carlo algorithm

We perform standard path integral Monte Carlo simulations on a finite lattice of size $N_s^2 \times N_\tau$, where N_s is the number of lattice sites in the space direction and N_τ in the temporal direction, with spacing ratio $\Delta\tau = a_t/a_s$. By varying $\Delta\tau$ it is possible to change a_t , while keeping the spacing in the spatial direction fixed. The simulations were performed on lattices with $N_s = 16$ sites in each of the two spatial directions and $N_t = 16 - 64$ in the temporal direction for a range of couplings $\beta = 1 - 3$.

The ensembles of field configurations were generated by using a Metropolis algorithm. Starting from an arbitrary initial configuration of link angles, we successively update link angles $\theta_\mu(\vec{r}, \tau)$ at positions (\vec{r}, τ) which are chosen randomly each time. We propose a change $\Delta\theta$ to this link angle, which is randomly drawn from a uniform distribution on $[-\Delta, \Delta]$, where Δ is adjusted for each set of parameters to give an acceptable “hit rate” around 70-80%. The change is accepted or rejected according to the standard Metropolis procedure.

For high anisotropy ($\Delta\tau \ll 1$), any change in a time-like plaquette will produce a large change in the action, whereas changes to the space-like plaquettes will cause a much smaller change in the action. This makes the system very “stiff” against variations in the time-like plaquettes, and therefore very slow to equilibrate, with long autocorrelation times. To alleviate this problem, we used a Fourier update procedure [41,42]. Here proposed changes are made to space-like links which are designed to alter space-like plaquette values much more than the time-like plaquette values. At randomly chosen intervals and random locations, we propose a non-local change $\Delta\theta(\vec{r}, \tau) = X \sin k(\tau - \tau_0)$ on a “ladder” of space-like links extending half a wavelength ($\lambda = 2\pi/k$) in the time direction, where both k and X are randomly chosen at each update from uniform distributions in suitably chosen intervals. We replaced approximately 30% of the ordinary Metropolis updates with Fourier updates for anisotropy $\Delta\tau > 0.444$ and 50% for highly anisotropic cases ($\Delta\tau < 0.444$). These moves satisfy the requirements of detailed balance and ergodicity for the algorithm.

A single sweep involves attempting N changes to randomly chosen links of the lattice, where $N (= 3N_t N_s^2)$ is the total number of links on the lattice. The first several thousand sweeps are discarded to allow the system to relax to equilibrium. Figure 1 shows measurements of the mean plaquette for $\beta = 2.0$ and $\Delta\tau = 1.0$, and it can be seen that equilibrium is reached after about 50,000 sweeps, with the measurements fluctuating about the equilibrium value thereafter. For highly anisotropic cases the system was much slower to equilibrate,

despite the Fourier acceleration, and in the worst case the equilibration time was of order 100,000 sweeps.

After discarding the initial sweeps, the configurations were stored every 250 sweeps thereafter for later analysis. Ensembles of about 1,000 configurations were stored to measure the static quark potential and glueball masses at each β for $\Delta\tau \geq 0.4$, and 1,400 configurations for $\Delta\tau \leq 0.333$. Measurements made on these stored configurations were grouped into 5 blocks, and then the mean and standard deviation of the final quantities were estimated by averaging over the ‘block averages’, treated as independent measurements. Each block average thus comprised 50,000 - 70,000 sweeps.

B. Interquark Potential

The static quark-antiquark potential, $V(\mathbf{r})$ for various spatial separations \mathbf{r} is extracted from the expectation values of the Wilson loops. The timelike Wilson loops are expected to behave as:

$$W(\mathbf{r}, \tau) \simeq Z(\mathbf{r}) \exp[-\tau V(\mathbf{r})] + (\text{excited state contributions}) \quad (14)$$

We have averaged only over loops $(\mathbf{x}_0, \tau_0) \rightarrow (\mathbf{x}_0 + \mathbf{r}, \tau_0) \rightarrow (\mathbf{x}_0 + \mathbf{r}, \tau_0 + \tau) \rightarrow (\mathbf{x}_0, \tau_0 + \tau) \rightarrow (\mathbf{x}_0, \tau_0)$ which follow either two sides of a rectangle between \mathbf{x}_0 and $\mathbf{x}_0 + \mathbf{r}$ or a single-step ‘staircase’ route, to estimate $W(\mathbf{r}, \tau)$. To suppress the excited state contributions, a simple APE smearing technique [43,44] was used on the space-like variables. In this technique an iterative smearing procedure is used to construct Wilson loop (and glueball) operators with a very high degree of overlap with the lowest-lying state. In our single-link smoothing procedure, we replace every space-like link variable by

$$U_i \rightarrow P \left[\alpha U_i + \frac{(1 - \alpha)}{2} \sum_s U_s \right] \quad (15)$$

where the sum over “s” refers to the “staples”, or 3-link paths bracketing the given link on either side in the spatial plane, and P denotes a projection onto the group $U(1)$, achieved by renormalizing the magnitude to unity. We used a smearing parameter $\alpha = 0.7$ and up to ten iterations of the smearing process.

To further reduce the statistical errors, the timelike Wilson loops were constructed from “thermally averaged” temporal links [45]. That is, the temporal links U_t in each Wilson loop were replaced by their thermal averages

$$\bar{U}_t = \int dU U \exp(-S[U]) / \int dU \exp(-S[U]) \quad (16)$$

where the integration is done over the one link only, and depends on the neighbouring links. For the $U(1)$ model, the result can easily be computed in terms of Bessel functions involving the ‘staples’ adjacent to the link in question. This was done for all temporal links except those adjacent to the spatial legs of the loop, which are not ‘independent’ [45]. The procedure has a dramatic effect in reducing the statistical noise, by up to an order of magnitude [4], worth a factor of 100 in Monte Carlo runtime.

The Wilson loop values $W(\mathbf{r}, \tau)$ are expected to decrease exponentially with Euclidean time τ . An ‘effective’ potential can be found from the ratios of successive loop values:

$$V(\mathbf{r}) = \frac{1}{\Delta\tau} \ln \left[\frac{W(\mathbf{r}, \tau + \Delta\tau)}{W(\mathbf{r}, \tau)} \right] \quad (17)$$

A typical plot of these estimates is shown in Figure 2 for $\beta = 2.0$, $\Delta\tau = 1.0$ and $R = \|\mathbf{r}\| = 4$. It can be seen that with the heavy smearing we have used, a flat ‘plateau’ is attained virtually straight away. We used $\tau = 1$ to make our estimates of $V(\mathbf{r})$.

C. Glueball masses

Estimates for the glueball masses were obtained from the time-like correlations between spatial Wilson loop operators $\Phi_i(\tau)$,

$$C(\tau) = \langle \Phi_i(\tau)^\dagger \Phi_i(\tau) \rangle \quad (18)$$

in a standard fashion. As the temporal separation becomes large, the above correlator tends to be dominated by the lowest energy state carrying the quantum numbers of Φ . If these quantum numbers coincide with those of the vacuum state, one then looks at the next higher energy state. So before taking the large Euclidean time limit, one subtracts the vacuum contribution from the correlator. Thus

$$\bar{\Phi}_i(\tau) = \Phi_i(\tau) - \langle 0 | \Phi_i(\tau) | 0 \rangle \quad (19)$$

is a gauge invariant, translationally invariant, vacuum-subtracted operator capable of creating a glueball out of the vacuum. As a function of the temporal separation τ , and with periodic boundary conditions, the correlation function is expected to behave as

$$\begin{aligned} C(\tau) &= \langle \bar{\Phi}_i^\dagger(\tau) \bar{\Phi}_i(0) \rangle \\ &\simeq c_0 + c_1 (\exp(-m_i(\tau)) + \exp(-m_i(T - \tau))) \\ &\quad + (\text{excited state contributions}) \end{aligned} \quad (20)$$

where m_i is the mass of the lowest glueball state in that sector, and $T = N_\tau a_t$ is the extent of the periodic lattice in the time direction. Note that the (negative) constant c_0 must be included because there is a sum rule that the sum of the vacuum-subtracted correlation function over all times must vanish. We project out states with momentum $\mathbf{k} = 0$ and spin $J = 0$ by summing over all lattice translations and rotations of the operators involved in Φ_i . In the present case, we study only the lowest-lying ‘antisymmetric’ (PC = - -) and ‘symmetric’ (PC = + +) glueball states, corresponding to operators Φ_i which are the sine and cosine, respectively, of the sum of the link angles around the Wilson loop in question.

The statistical fluctuations in $C(\tau)$ are given by [46]

$$\sigma \rightarrow \frac{C(0)}{\sqrt{N}} \quad (21)$$

Thus, the signal-to-noise ratio collapses as $C(\tau)$ falls exponentially fast with τ . Hence, it becomes important to use a glueball operator for which the overlap with the glueball state

of interest is strong for small lattice spacing, and such that $C(\tau)$ attains its asymptotic form as quickly as possible. For such an operator, the signal-to-noise ratio is also optimal [46]. Such operators can be constructed by exploiting link smearing and variational techniques [4,47].

In the strong coupling limit $\beta = 0$, the plaquette operator U_P will create a symmetric glueball state from the vacuum. For large β , however, the glueball wave functions are expected to spread out and become more diffuse. To obtain a good overlap with the ground state in each sector at weak coupling, we need large, smooth operators ϕ_i on the lattice scale. An optimized operator is found by a variational technique, following Morningstar and Peardon [4] and Teper [47]. First, we calculate the correlation functions for square $n \times n$ Wilson loops with m smearings, and determine the values of m and n for which the ratio $(C(1)/C(0))_{nm}$ is a maximum. In the second pass, an optimized glueball operator was found as a linear combination of the basic operators ϕ_i ,

$$\Phi(\tau) = \sum_{\alpha} v_{i\alpha} \phi_{i\alpha}(\tau) \quad (22)$$

where the index α runs over the rectangular Wilson loops with dimensions $l_x = [n-1, n+1]$, $l_y = [n-1, n+1]$ and smearings $n_s = [m-1, m+1]$ with n and m as determined in the first pass, making 27 operators in all. The 27×27 correlation matrix was computed

$$C_{i\alpha\beta}(\tau) = \sum_{\tau_0} \langle 0 | \bar{\phi}_{i\alpha}(\tau + \tau_0) \bar{\phi}_{i\beta}(\tau_0) | 0 \rangle \quad (23)$$

where $\bar{\phi}_{i\alpha}(\tau)$ is a vacuum-subtracted operator

$$\bar{\phi}_{i\alpha}(\tau) = \phi_{i\alpha}(\tau) - \langle 0 | \phi_{i\alpha}(\tau) | 0 \rangle$$

The coefficients $v_{i\alpha}$ were then determined by minimizing the effective mass at $\tau = 1$

$$\tilde{m}(1) = -\frac{1}{a_t} \ln \left[\frac{\sum_{\alpha\beta} v_{i\alpha} v_{i\beta} C_{i\alpha\beta}(1)}{\sum_{\alpha\beta} v_{i\alpha} v_{i\beta} C_{i\alpha\beta}(0)} \right] \quad (24)$$

Let \mathbf{v}_i denote a column vector whose elements are the optimal values of the coefficients $v_{i\alpha}$, then the column vector \mathbf{v}_i formed from the $v_{i\alpha}$ is the solution of an eigenvalue equation

$$C(1)\mathbf{v}_i = e^{-a_t \tilde{m}(1)} C(0)\mathbf{v}_i \quad (25)$$

The eigenvector \mathbf{v}_0 corresponding to the largest eigenvalue $e^{-a_t \tilde{m}}$ then yields the coefficients for the operator $\Phi_i(\tau)$ which best overlaps the lowest-lying state.

A third pass was made to estimate the optimized correlation function

$$C_i(\tau) = \sum_{\tau_0} \langle 0 | \bar{\Phi}_i(\tau + \tau_0) \bar{\Phi}_i(\tau_0) | 0 \rangle \quad (26)$$

Finally the optimized correlation function was fitted with the simple form

$$C_i(\tau) = c_0 + c_1 \cosh m_i \left(\frac{T}{2} - \tau \right) \quad (27)$$

to determine the glueball mass estimates. Figure 3 shows an example of the correlation function and fit for the antisymmetric state at $\beta = 2$ and $\Delta\tau = 1$. It can be seen that the form (27) fits the data very well.

IV. SIMULATION RESULTS AT FINITE LATTICE SIZE

Simulations were carried out for lattices of $N_s^2 \times N_t$ sites, with $N_s = 16$ and N_t ranging from 16 to 48 sites, with periodic boundary conditions. Each run involved 250,000 sweeps (350,000 for high anisotropy) of the lattice, with 50,000 sweeps (100,000 high anisotropy) discarded to allow for equilibrium, and configurations recorded every 250 sweeps thereafter. Coupling values from $\beta = 1.0$ to 3.0 were explored at anisotropies $\Delta\tau$ ranging from 1 to 1/3. We fixed $\Delta\tau = 16/N_t$ in the first pass, so that the lattice size remains fixed at $16a_s$ in all directions. At strong couplings (small β), we expect the behaviour to be the same as in the bulk system, but at weaker couplings (large β) the finite-size/finite-temperature corrections will become more important. We shall monitor our data for signs of these effects.

A. Mean Plaquette

Figure 4 shows the behaviour of the mean spatial plaquette $\langle P \rangle$ for different β , at fixed $\Delta\tau = 1$ (Euclidean, isotropic case). A strong coupling perturbation series expansion has been obtained for this quantity by Bhanot and Creutz [48] to order β , and a weak coupling series to order $1/\beta^5$ by Horsley and Wolff [49]. These series are represented by solid and dashed lines on the graph, respectively. It can be seen that the data follow the strong-coupling expansion for $\beta \leq 1.5$, and match the weak-coupling expansion quite closely beyond $\beta \simeq 2$. The variation of $\langle P \rangle$ with coupling is extremely smooth, with no sign of any phase transition, as we should expect. The cross-over from strong to weak coupling seems to take place quite rapidly in the region $\beta \approx 1.8 - 2.0$. Horsley and Wolff [49] investigated the effect of a finite-size lattice in their weak-coupling expansion calculations. They found that such effects enter at order $1/\beta^2$ as a correction of order $1/L^D$, where L is the lattice size and D is the number of dimensions. Thus for the compact U(1) model in 3-dimensions and $L > 10$, the finite size effects should be essentially negligible.

Figure 5 shows a plot of our estimates of $\langle P \rangle$ as a function of anisotropy $\Delta\tau^2$ for the case $\beta = \sqrt{2}$. It can be seen that $\langle P \rangle$ remains almost constant. We would like to make contact with previous Hamiltonian studies by showing that the mean plaquette value approaches to previously known values in the Hamiltonian limit $\Delta\tau \rightarrow 0$. The extrapolation was performed using a simple cubic fit in powers of $\Delta\tau^2$. In this limit our results agree very well with the Hamiltonian estimate obtained by Hamer et al [19].

Figure 6 graphs the resulting estimates of $\langle P \rangle$ in the Hamiltonian limit $\Delta\tau = 0$ as a function of coupling β . The weak-coupling [40] and strong-coupling [30] series predictions are shown as dashed and solid lines on the graph respectively, while some previous Greens Function Monte Carlo estimates [19] are shown as triangles. Our present results are generally in reasonable agreement with the earlier ones, if perhaps a little low in places. It can be seen that the crossover from strong to weak coupling behaviour again occurs at around $\beta \simeq 1.8$.

B. Static quark potential and string tension

Figure 7 shows a graph of the static quark potential $V(R)$ as a function of radius R at $\beta = 2.0$ and $\Delta\tau = 1.0$. To extract the string tension, the curve is fitted by a form

$$V(R) = a + b \ln R + \sigma R, \quad (28)$$

including a logarithmic Coulomb term as expected for classical QED in (2+1) dimensions which dominates the behaviour at small distances, and a linear term as predicted by Polyakov [26] and Göpfert and Mack [27] dominating the behaviour at large distances. The linear behaviour at large distances is very clear, but the data do not extend to very small distances, so there is no real test of the presumed logarithmic behaviour in this regime.

Figure 8 shows the behaviour of the fitted value of the string tension $K = \sigma a^2$ as a function of β for the Euclidean, isotropic case ($\Delta\tau = 1$). The solid line on the graph represents the form (6) predicted by Göpfert and Mack [27], using a value of $c = 44 \pm 0.42$. It can be seen that this form represents the data rather well over a range $1.41 \leq \beta \leq 2.5$; in fact an unconstrained fit to the data gives a slope of 2.49 ± 0.15 , extremely close to the predicted value 2.494. The coefficient c , however, is much bigger than the value $c = 8$ predicted in the classical approximation. It would be interesting to explore how higher-order quantum corrections affect the prediction for c .

The dashed line in Figure 8 gives some idea of the expected finite-size scaling corrections to the string tension. These have not been calculated explicitly for the Euclidean model, as far as we are aware, but in the Hamiltonian version the string tension at weak coupling is found [40] to behave as

$$K = \frac{1}{2\beta L} \quad (29)$$

where $L = N_s$ is the lattice size (here $L = 16$), and this is represented by the dashed line. This would predict that the string tension will be dominated by finite-size corrections beyond $\beta \simeq 2.5$, and indeed the Monte Carlo estimates do flatten out beyond that point, although at a level below equation (29).

Figure 9 shows the behaviour of the string tension K as a function of the anisotropy $\Delta\tau^2$, for fixed coupling $\beta = \sqrt{2}$. An extrapolation to the Hamiltonian limit $\Delta\tau \rightarrow 0$ is performed by a simple cubic fit. Again the extrapolation agrees well with earlier Hamiltonian estimates [12]. Note that this quantity depends rather strongly on $\Delta\tau$: there is a factor of three difference between the values at $\Delta\tau = 0$ and $\Delta\tau = 1$. Extrapolating to $\Delta\tau \rightarrow 0$, estimates of the string tension in the Hamiltonian limit are obtained for various β values.

Our estimates of the string tension in the Hamiltonian limit are graphed in Figure 10, together with earlier results from an ‘exact linked cluster expansion’ [50] and a quantum Monte Carlo simulation [12]. It can be seen that our values are consistent with earlier results, though less accurate, and extend further into the weak-coupling region. The solid line in the graph represents a least-square fit of the weak-coupling asymptotic form (6), with $v(0) = 0.3214$ and $c = 46.67 \pm 0.37$. This form represents the data well for $1.35 \leq \beta \leq 2.0$. Beyond $\beta = 2$ the string tension is consistent, within errors, with the finite-size behaviour predicted by equation (29), which is shown as a dashed line.

C. Glueball Masses

Figure 11 shows results for the antisymmetric 0^{--} glueball mass against β for the isotropic Euclidean case $\Delta\tau = 1$. The solid line on the graph is a fit to the data over

the range $1.4 \leq \beta \leq 2.25$ using the predicted asymptotic form, equation (5), but with an additional multiplying constant:

$$M = am_D = c_1 \sqrt{8\pi^2 \beta} \exp(-\pi^2 \beta v(0)) \quad (30)$$

where $c_1 = 5.23 \pm 0.11$ when adjusted to fit the data. Thus the slope, 2.48 ± 0.09 , of the data matches the predicted asymptotic form very nicely, but the coefficient is too large by a factor of 5.2. It would again be interesting to explore whether this discrepancy could be due to quantum corrections.

The expected finite-size scaling behaviour of the mass gap near the continuum critical point in this model is not known; but Weigel and Janke [51] have performed a Monte Carlo simulation for an O(2) spin model in three dimensions which should lie in the same universality class, obtaining

$$M \sim 1.3218/L \quad (31)$$

for the magnetic gap. The dashed line in Figure 11 shows this prediction for $L = 16$. It can be seen that the Euclidean mass gap should not be affected by finite-size corrections until $\beta \geq 2.8$.

To check the consistency of our method, we plot the dimensionless ratio of the anti-symmetric mass gap over the square root of the string tension against β together with the results of Teper [47] in Figure 12. The agreement is excellent. The solid line gives the ratio of the fits in Figures 8 and 11, and shows how this ratio vanishes exponentially in the weak-coupling limit, whereas in four-dimensional confining theories it goes to a constant.

Figure 13 shows the behaviour of the glueball masses as functions of $\Delta\tau^2$ for $\beta = \sqrt{2}$. The extrapolation to the Hamiltonian limit is performed by a simple cubic fit in powers of $\Delta\tau^2$. In this limit we reproduce the earlier estimates of Hamer et al [30] for the 0^{--} and 0^{++} states.

Estimates of the antisymmetric mass gap in the Hamiltonian limit $\Delta\tau = 0$ are graphed against β in Figure 14. Also shown are results from previous strong-coupling series extrapolations [30] and quantum Monte Carlo calculations [12]. It can be seen that our present results agree with previous estimates but are less accurate. The solid line is a fit to the data for $1.4 \leq \beta \leq 2.25$ of the form (27), with $v(0) = 0.3214$ and $c_1 = 5.50 \pm 0.24$, which is similar to the coefficient found in the Euclidean case. The fitting parameters, the slope 3.10 ± 0.16 and the intercept 3.61 ± 0.26 of the scaling curve, are in excellent agreement with the results obtained from the other Hamiltonian studies, tabled in [17] and the references therein. The dashed line represents the finite-size scaling behaviour, equation (31), which we assume holds in the Hamiltonian limit also, for want of better information. It can be seen that the finite-size corrections are predicted to dominate for $\beta \geq 2.2$, but the date are not accurate enough at weak couplings to establish whether this is really the case.

Finally, Figure 15 displays the behaviour of the dimensionless mass ratio,

$$R_M = M(0^{++})/M(0^{--}) \quad (32)$$

for the Euclidean case $\Delta\tau = 1$. As in the (3+1)D confining theories, we may expect that quantities of this sort will approach their weak-coupling or continuum limits with corrections of $O(1/a_{eff})$, where a_{eff} is the effective lattice spacing in ‘physical’ units when the mass gap

has been renormalized to a constant. Hence for our present purposes we *define* a_{eff} from equation (5) as

$$a_{eff} = \sqrt{8\pi^2\beta} \exp(-\pi^2\beta v(0)) \quad (33)$$

with $v(0) = 0.2527$ for the Euclidean case. The mass ratio is plotted against a_{eff} in Figure 15. At weak coupling, we expect the theory to approach a theory of free bosons [27] so that the symmetric state will be composed of two 0^{--} bosons and the mass ratio should approach two. Our results show that as a_{eff} goes to zero, the mass ratio rises to around the expected value of 2.0. A linear fit to the data from $0.08 \leq a_{eff} \leq 0.35$ gives an intercept $R_M = 1.91 \pm 0.05$. However, we note that the last one of our estimates, together with two from Teper [47], lie considerably *above* $R_M = 2$. In the block systems, of course, the ratio cannot rise above 2, because it is always possible to construct a 0^{++} state out of two 0^{--} mesons. These points correspond to couplings $\beta > 2$, and we conjecture that they may be affected by finite-size corrections: a simulation on a larger lattice would be necessary to check on this point. This last point has not been included in the fit.

Figure 16 shows a similar graph for the Hamiltonian limit, $\Delta\tau = 0$. Within errors, our present results are consistent with earlier series [30] and quantum Monte Carlo [12] estimates, but considerably less accurate, and tend to lie consistently on the high side. A linear fit to the earlier data from $0.02 \leq a_{eff} \leq 0.12$ gives $R_M = 2.14$.

V. CONCLUSIONS

In this paper, we have applied standard Euclidean path integral Monte Carlo methods to the U(1) model in (2+1) dimensions on an anisotropic lattice, and taken the anisotropic limit $\Delta\tau \rightarrow 0$ to obtain the Hamiltonian limit of the model.

We have obtained the first clear picture of the static quark potential in this model, showing very clear evidence of the linear confining behaviour at large distances predicted by Polyakov [26]. There is also a turnover at short distances consistent with a logarithmic Coulomb behaviour in that regime.

In the isotropic or Euclidean case $\Delta\tau = 1$, the string tension and mass gap display an exponential decrease at weak couplings which is in excellent agreement with the behaviour predicted by Polyakov [26] and Göpfert and Mack [27]. Both quantities, however, are 5-6 times larger in magnitude than the theory predicts. It would be interesting to calculate whether higher-order quantum corrections can account for this discrepancy.

The dimensionless ratio M/\sqrt{K} scales exponentially to zero in the weak-coupling or continuum limit, as predicted by the theory. The mass ratio of the two lowest glueball states scales against the effective lattice spacing towards a value close to 2.0, as expected for a theory of free scalar bosons, apart from some anomalous results at large β which we have ascribed to finite-lattice effects.

In the anisotropic or Hamiltonian limit $\Delta\tau \rightarrow 0$, our results are less accurate, because of the extrapolation needed to reach this limit. Nevertheless, the results are generally in good agreement with those obtained by other methods. Once again, an exponential behaviour of the string tension and glueball masses can be demonstrated at weak coupling. The dimensionless mass ratio again scales to a value near 2.0. Because the exponential slope is

steeper, finite-size effects seem to be somewhat more important in the Hamiltonian regime than in the Euclidean one.

Our major object in this study was to compare the Euclidean PIMC approach to quantum Monte Carlo methods such as Green's Function Monte Carlo (GFMC) for obtaining estimates in the Hamiltonian limit. The PIMC approach suffers from the disadvantage that an extrapolation is necessary to reach the limit $\Delta\tau \rightarrow 0$; while GFMC suffers from the major disadvantage that it relies on a ‘trial wave function’. In the event, we have obtained much better results using PIMC. A clear and consistent picture of the string tension and glueball masses was obtained at weak coupling. Using GFMC, on the other hand, only qualitative estimates of the string tension were obtained, and the glueball mass estimates were virtually worthless [19]. No doubt there are many ‘tricks of the trade’, such as smearing and variational techniques, which could be used to improve the GFMC results; but we found previously [20] that there is an unacceptably strong dependence on the trial wave function using that technique, especially for large lattice size. The PIMC technique seems to offer a much more robust and unbiased approach to Hamiltonian lattice gauge theories. Of course, one must generally expect the Hamiltonian estimates to be less accurate than the Euclidean ones because of the extra extrapolation involved.

We note that the PIMC results are still less accurate than some older quantum Monte Carlo results of Hamer, Wang and Price [12]. The latter were obtained using a strong-coupling representation, however, and this approach has been found to fail for non-Abelian models [12] due to the occurrence of a ‘minus sign’ problem, as mentioned in the introduction.

ACKNOWLEDGMENTS

This work was supported by the Australian Research Council. We are grateful to Mr. Tim Byrnes for help with some of the calculations. We are also grateful for access to the computing facilities of the Australian Centre for Advanced Computing and Communications (ac3) and the Australian Partnership for Advanced Computing (APAC).

REFERENCES

- [1] M. Creutz, Phys. Rev. Letts. **43**, 553 (1979)
- [2] K.G. Wilson, Phys. Rev. **D10**, 2445 (1974)
- [3] J. Kogut and L. Susskind, Phys. Rev. **D11**, 395 (1975)
- [4] C.J. Morningstar and M. Peardon, Phys. Rev. **D56**, 4043 (1997)
- [5] C. J. Hamer, M. Sheppeard, W. H. Zheng and D. Schütte, Phys. Rev. **D54**, 2395 (1996)
- [6] T.Banks, S. Raby, L. Susskind, J. Kogut, D.R.T. Jones, P.N. Scharbach and D.K. Sinclair, Phys. Rev. **D15**, 1111 (1977)
- [7] D. Horn and M. Weinstein, Phys. Rev. **D30**, 1256 (1984)
- [8] Guo Shuhong, Zheng Weihong and Liu Jiunmin, Phys. Rev. **D38**, 2591 (1988)
- [9] T.M.R. Byrnes, P.Sriganesh, R.J. Bursill and C.J. Hamer, to be published in Phys. Rev. D
- [10] D. Blankenbecler and R.L. Sugar, Phys. Rev. **D27**, 1304 (1983)
- [11] T.A. DeGrand and J. Potvin, Phys. Rev. **D31**, 871 (1985)
- [12] C. J. Hamer, K. C. Wang and P. F. Price, Phys. Rev. **D50**, 4693 (1994)
- [13] S. A. Chin, J. W. Negele and S. E. Koonin, Ann. Phys. (N.Y.) **157**, 140 (1984)
- [14] D. W. Heys and D. R. Stump, Phys. Rev. **D28**, 2067 (1983)
- [15] Kalos M. H., J. Comp. Phys. **1**, 257 (1966); D. M. Ceperley and M. H. Kalos, in *Monte Carlo Methods in Statistical Mechanics*, ed. K. Binder (Springer-Verlag, New York, 1979).
- [16] M. Samaras and C. J. Hamer, Aust. J. Phys. **52**, 637 (1999)
- [17] J. McIntosh and L. Hollenberg, Z. Phys. **C76**, 175 (1997)
- [18] M.N. Chernodub, E.-M. Ilgenfritz and A. Schiller, Phys. Rev. **bf 64D**, 054507 (2001)
- [19] C.J. Hamer, R.J. Bursill and M. Samaras, Phys. Rev. **D62**, 054511 (2000)
- [20] C.J. Hamer, R.J. Bursill and M. Samaras, Phys. Rev. **D62**, 074506 (2000)
- [21] K.S. Liu, M.H. Kalos and G.V. Chester, Phys. Rev. **A10** 303 (1974)
- [22] P. A. Whitlock, D. M. Ceperley, G. V. Chester and M. H. Kalos, Phys. Rev. **B19**, 5598 (1979)
- [23] J. Ambjorn, A.J.G. Hey and S. Otto, Nucl. Phys. **B210**, 347 (1982)
- [24] P.D. Coddington, A.J.G. Hey, A.A. Middleton and J.S. Townsend, Phys. Letts. **B175**, 64 (1986)
- [25] L. Gross, Commun. Math. Phys. **92**, 137 (1983)
- [26] A.M. Polyakov, Phys. Lett. **72B**, 477 (1978)
- [27] M. Göpfert and G. Mack, Commun. Math. Phys. **82**, 545 (1982)
- [28] T. Banks, R. Myerson and J. Kogut, Nucl. Phys. **B129**, 493 (1977).
- [29] S. Ben-Menahem, Phys. Rev. **bf D20**, 1923 (1979).
- [30] C. J. Hamer, J. Oitmaa, and Zheng Weihong, Phys. Rev. **D45**, 4652 (1992)
- [31] C.J.Hamer, Zheng Weihong and J. Oitmaa, Phys. Rev. **D53**, 1429 (1996)
- [32] A.C. Irving, J.F. Owens and C.J.Hamer, Phys. Rev. **D28**, 2059 (1983)
- [33] D. Horn, G. Lana and D. Schreiber, Phys. Rev. **D36**, 3218 (1987)
- [34] C.J. Morningstar, Phys. Rev. **D46**, 824 (1992)
- [35] A. Dabringhaus, M.L. Ristig and J.W. Clark, Phys. Rev. **D43**, 1978 (1991)
- [36] X.Y. Fang, J.M. Liu and S.H. Guo, Phys. Rev. **D53**, 1523 (1996)
- [37] S.J. Baker, R.F. Bishop and N.J. Davidson, Phys. Rev. **D53**, 2610 (1996).
- [38] S. E. Koonin, E. A. Umland and M. R. Zirnbauer, Phys. Rev. **D33**, 1795 (1986)

- [39] C. M. Yung, C. R. Allton and C. J. Hamer, Phys. Rev. **D33**, 1795 (1986)
- [40] C. J. Hamer and Zheng Weihong, Phys. Rev. **D48**, 4435 (1993)
- [41] G.G. Batrouni, G.R. Katz, A.S. Kronfeld, G.P. Lepage, B.Svetitsky and K.G. Wilson, Phys. Rev. **D32**, 2736 (1985)
- [42] C.T.H. Davies, G.G. Batrouni, G.R. Katz, A.S. Kronfeld, G.P. Lepage, P. Rossi, B. Svetitsky and K.G. Wilson, Phys. Rev. **D41**, 1953 (1990)
- [43] M. Albanese *et al.*, Phys. Lett. **B192**, 163 (1987)
- [44] M. Teper, Phys. Lett. **B183**, 345 (1986); K.Ishikawa, A. Sato, G. Schierholz and M. Teper, Z. Phs. **C21**, 167 (1983)
- [45] G. Parisi, R. Petronzio and F. Rapuano, Phys. Lett. **128B**, 418 (1983)
- [46] F. Brandstaeter *et al.*, Nucl.Phys. **B345**, 709 (1990)
- [47] M.J. Teper, Phys. Rev. **D59**, 014512 (1999)
- [48] G. Bhanot and M. Creutz, Phys. Rev. **D21**, 2892 (1980)
- [49] R. Horsley and U. Wolff, Phys. Letts. **B105**, 290 (1981)
- [50] A.C. Irving and C.J. Hamer, Nucl. Phys. **B235**, 358 (1984)
- [51] M. Weigel and W. Janke, Phys. Rev. Letts. **82**, 2318 (1999)

FIGURES

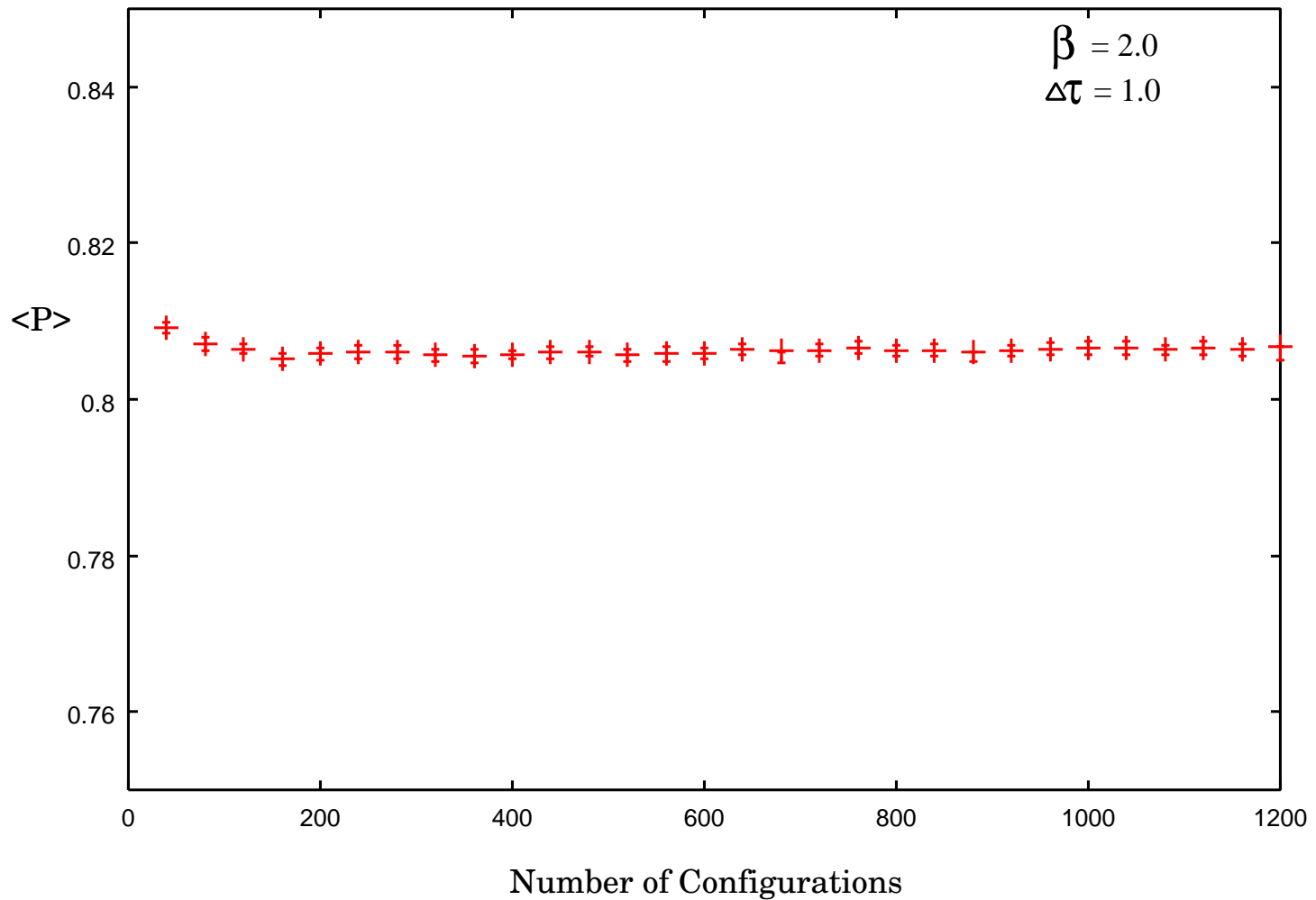


FIG. 1. Plot of the mean plaquette value against the number of configurations.

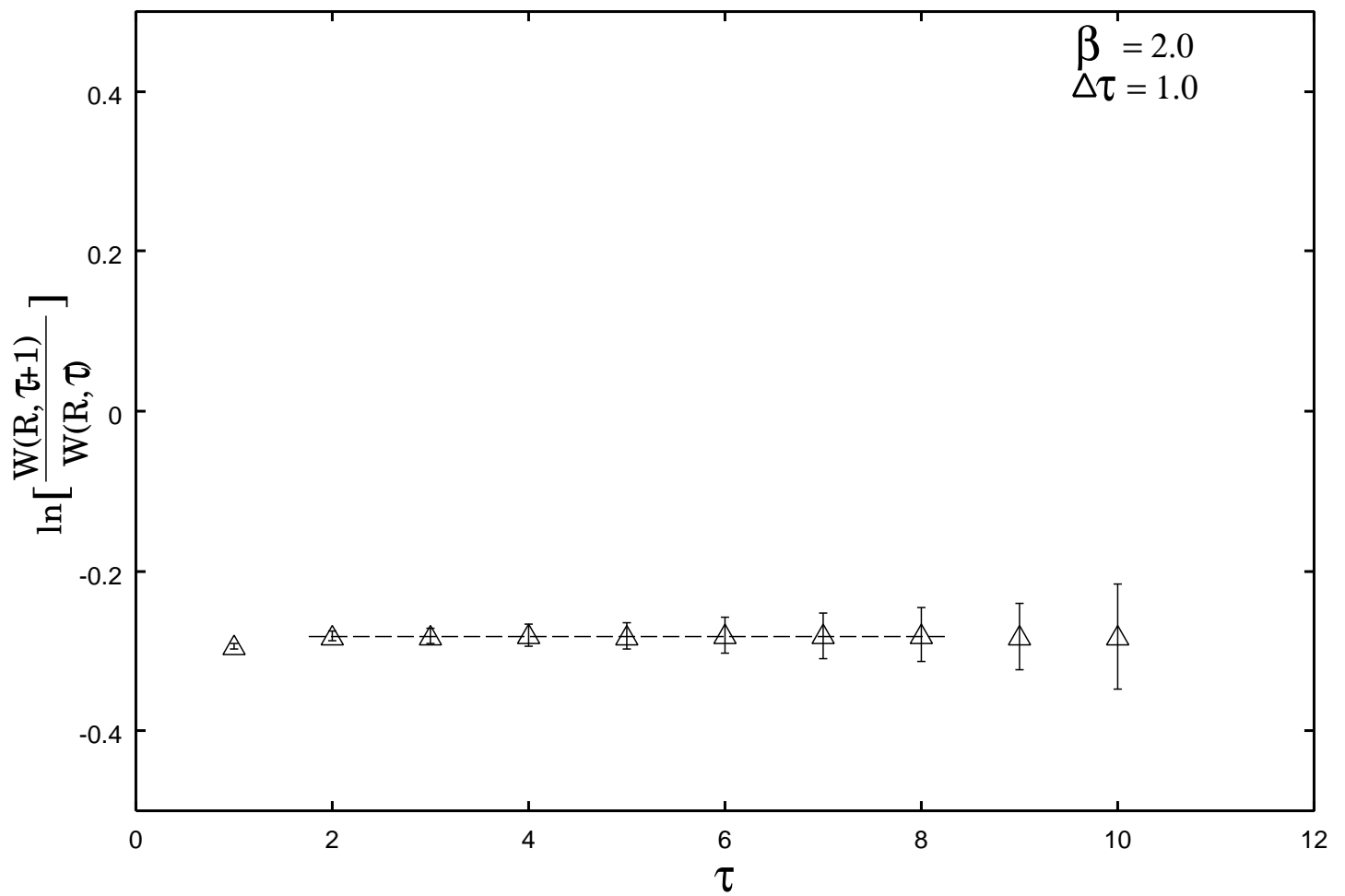


FIG. 2. Logarithmic ratio of Wilson loops as a function of τ for fixed $R = 4$ at $\beta = 2.0$ and $\Delta\tau = 1.0$. The dashed horizontal line indicates the plateau value.

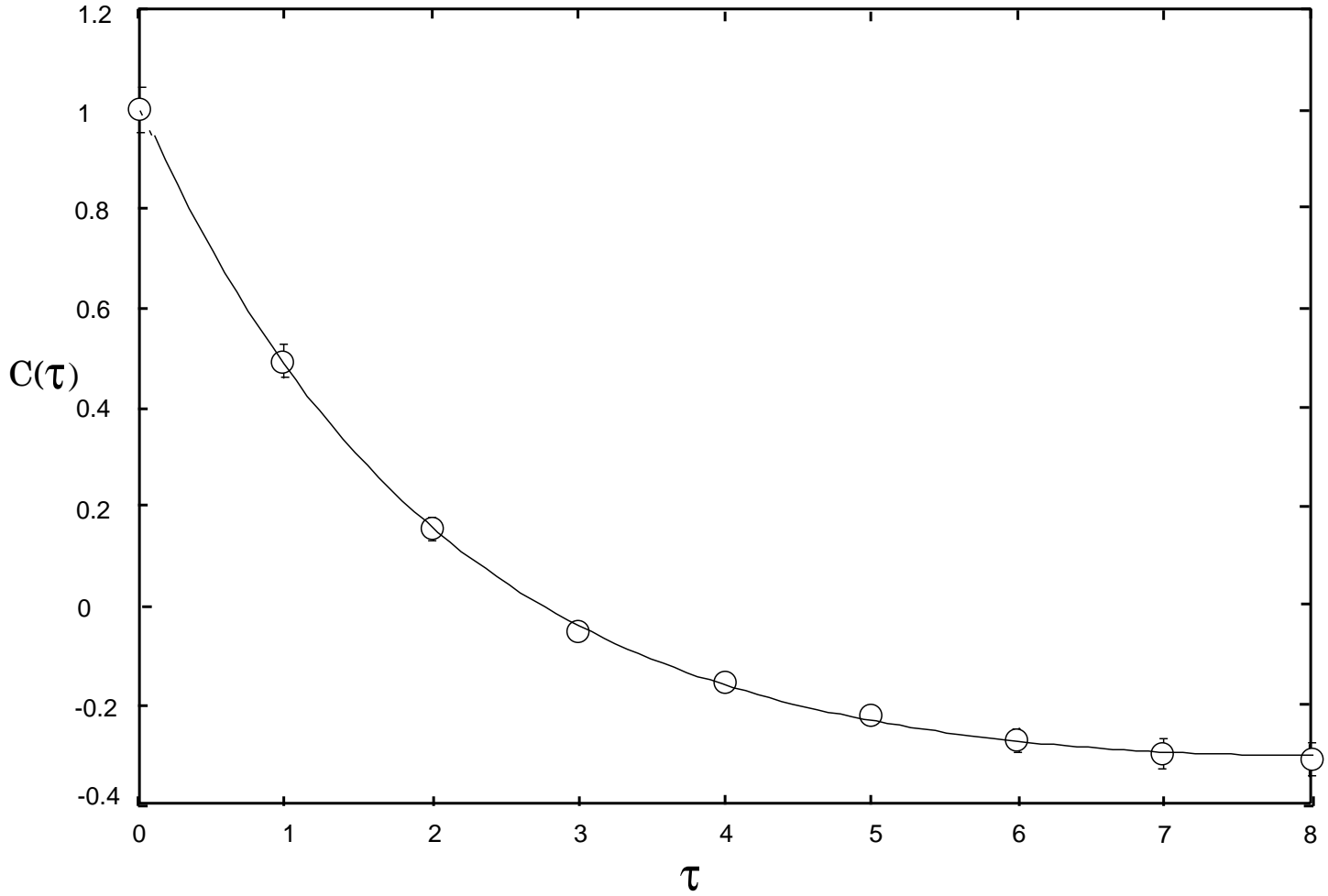


FIG. 3. Antisymmetric glueball correlation function $C(\tau)$ for the 0^{--} channel against τ at $\Delta\tau = 1.0$ and $\beta = 2.0$. The solid curve is a fit to the simulation results using Eq. (27).

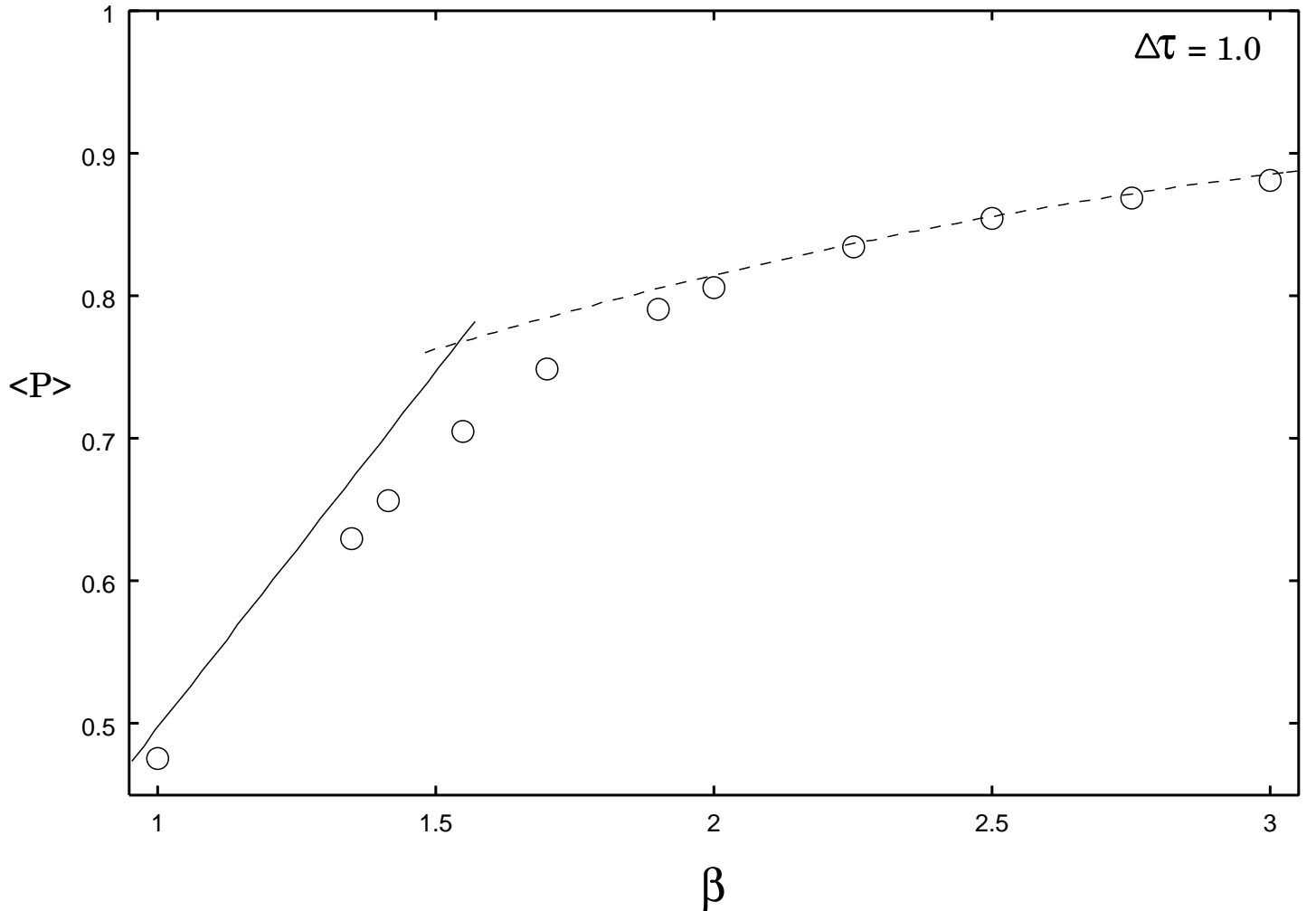


FIG. 4. The mean plaquette as a function of β at $\Delta\tau = 1$. The circles are our Monte Carlo estimates. The solid curve represents the $O(\beta)$ strong-coupling expansion [48] and the dashed curve represents the $O(1/\beta^4)$ weak-coupling expansion [49].

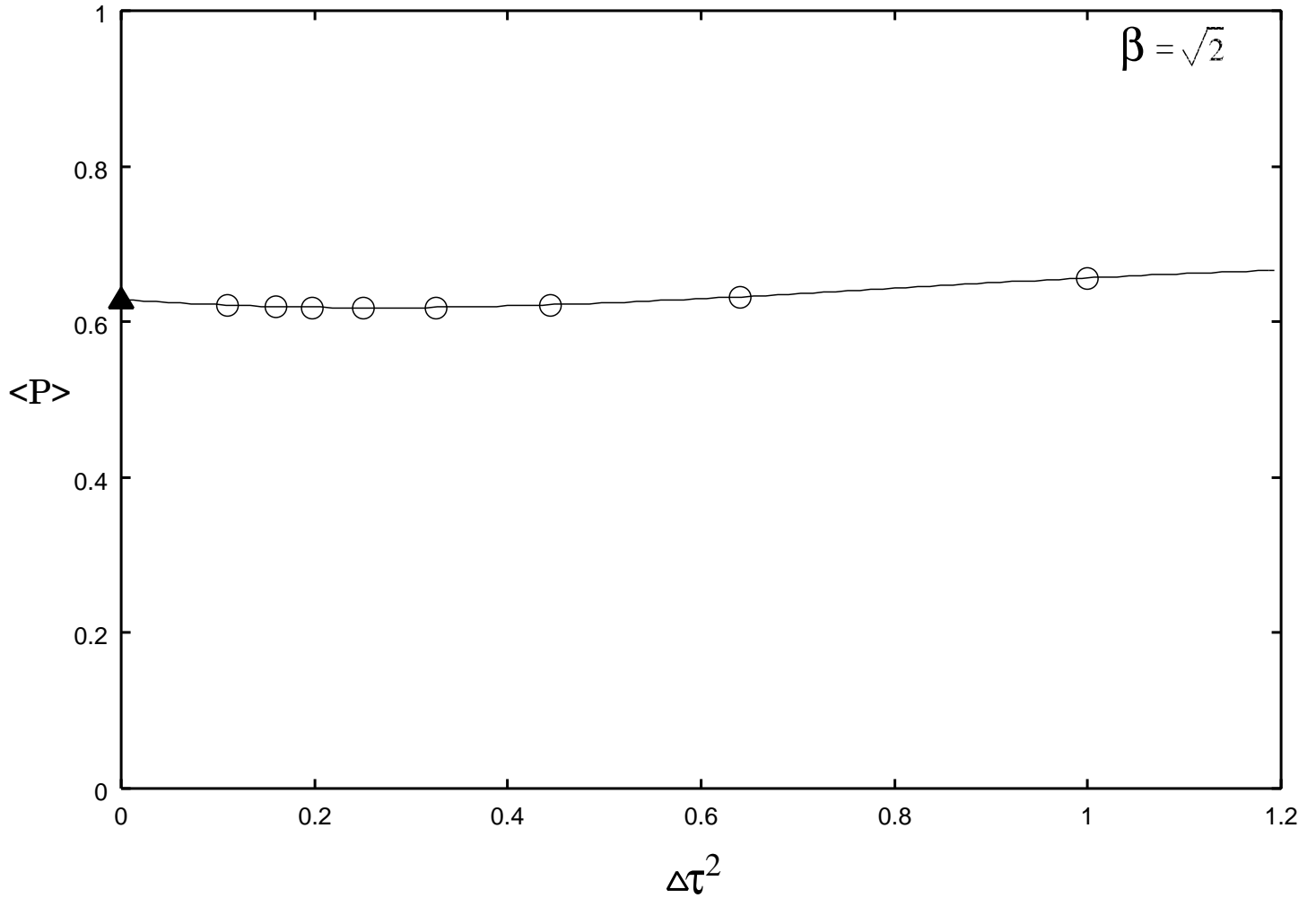


FIG. 5. The mean plaquette as a function of $\Delta\tau^2$ at $\beta = \sqrt{2}$. The solid curve is a cubic fit to the data, extrapolated to the Hamiltonian limit. The triangle shows the Hamiltonian series estimate [19] in that limit.

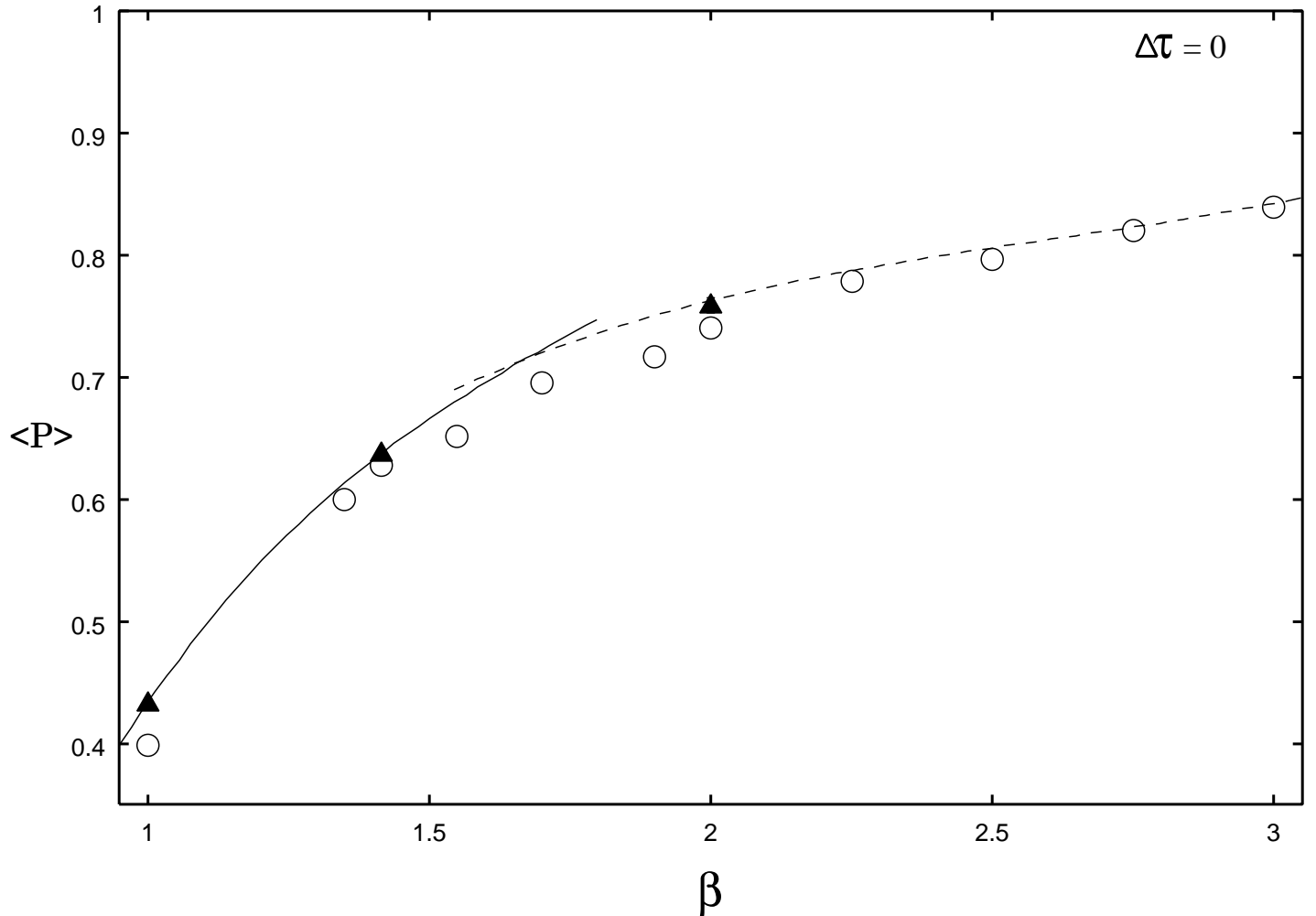


FIG. 6. Mean plaquette estimates as a function of β at $\Delta\tau = 0$. Our present Monte Carlo estimates are shown by circles. The strong-coupling [30] and weak-coupling [40] series predictions are shown as solid and dashed lines respectively. The GFMC estimates [19] are represented by the solid triangles.

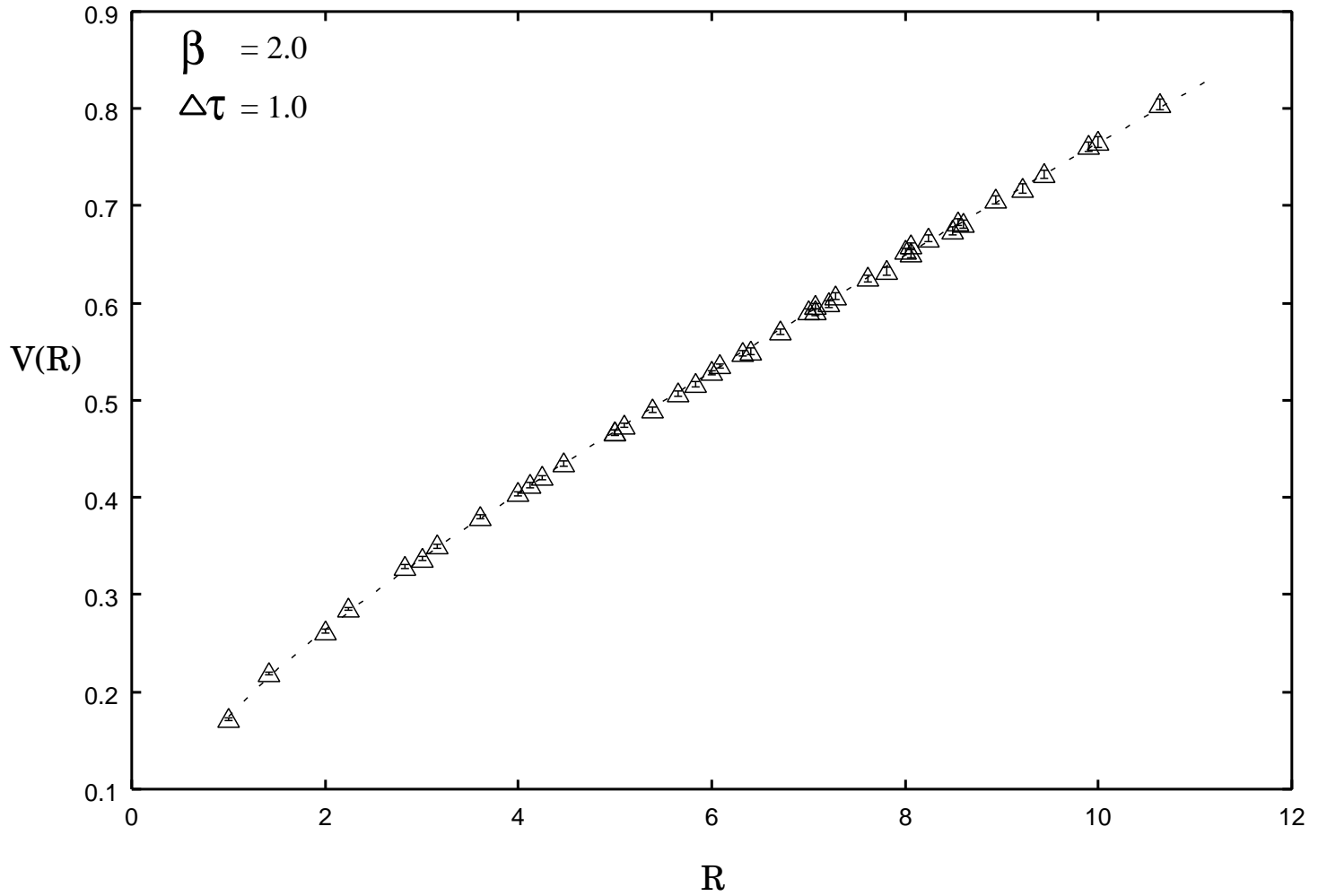


FIG. 7. The static-quark potential $V(R)$ as a function of the separation R . This plot involves measurements at $\beta = 2.0$ for $\Delta\tau = 1.0$ with 10 smearing sweeps at smearing parameter $\alpha = 0.7$. The errors are smaller than the symbols. The dashed line is a fit to the form $V(R) = a + bR + c\ln(R)$.

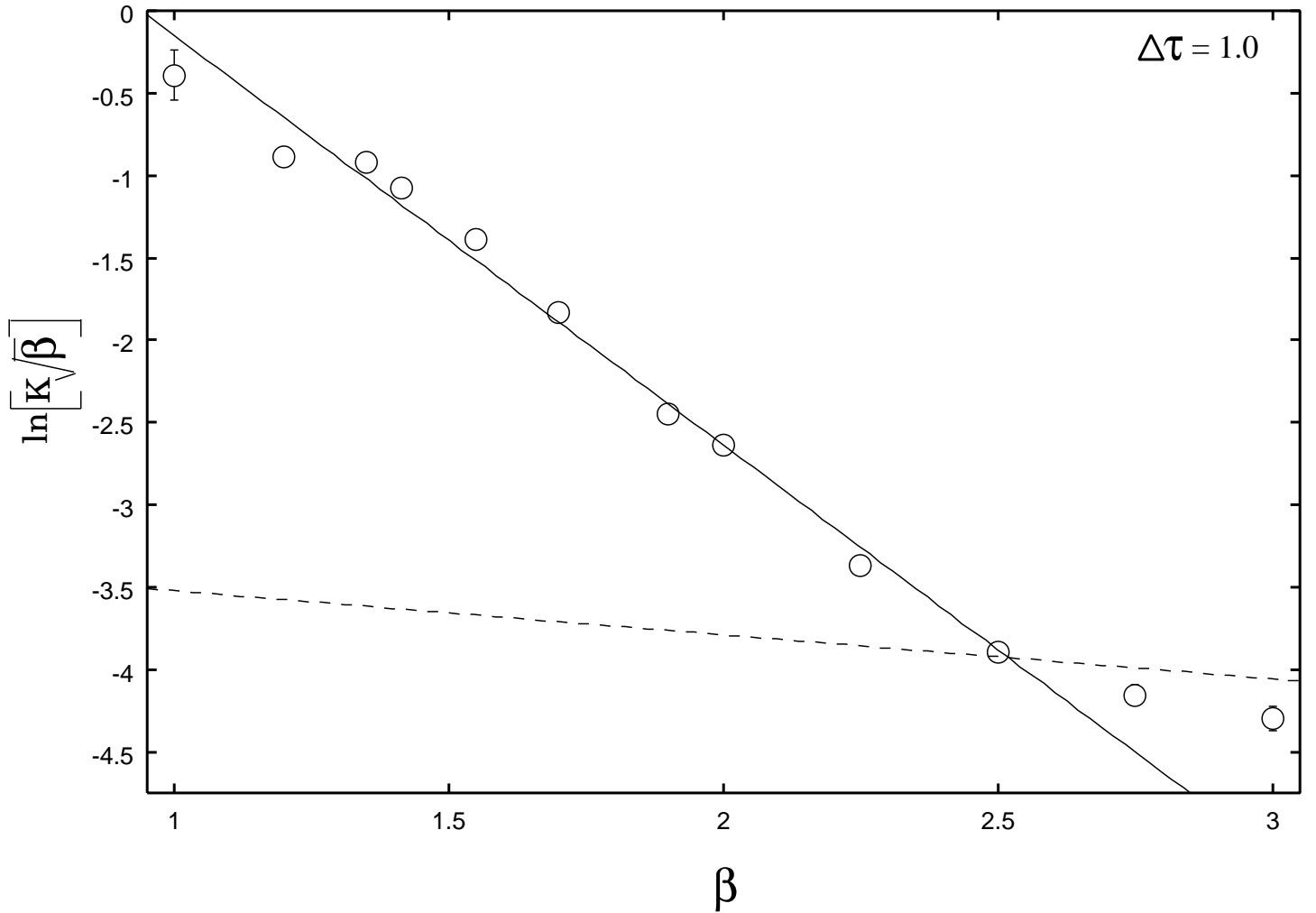


FIG. 8. $\ln(K\sqrt{\beta})$ as a function of β at $\Delta\tau = 1.0$. The solid curve represents the predicted asymptotic form, eq. (6), with our estimated value for the normalization constant, $c = 44 \pm 0.42$. The dashed line represents the finite size scaling behaviour [40].

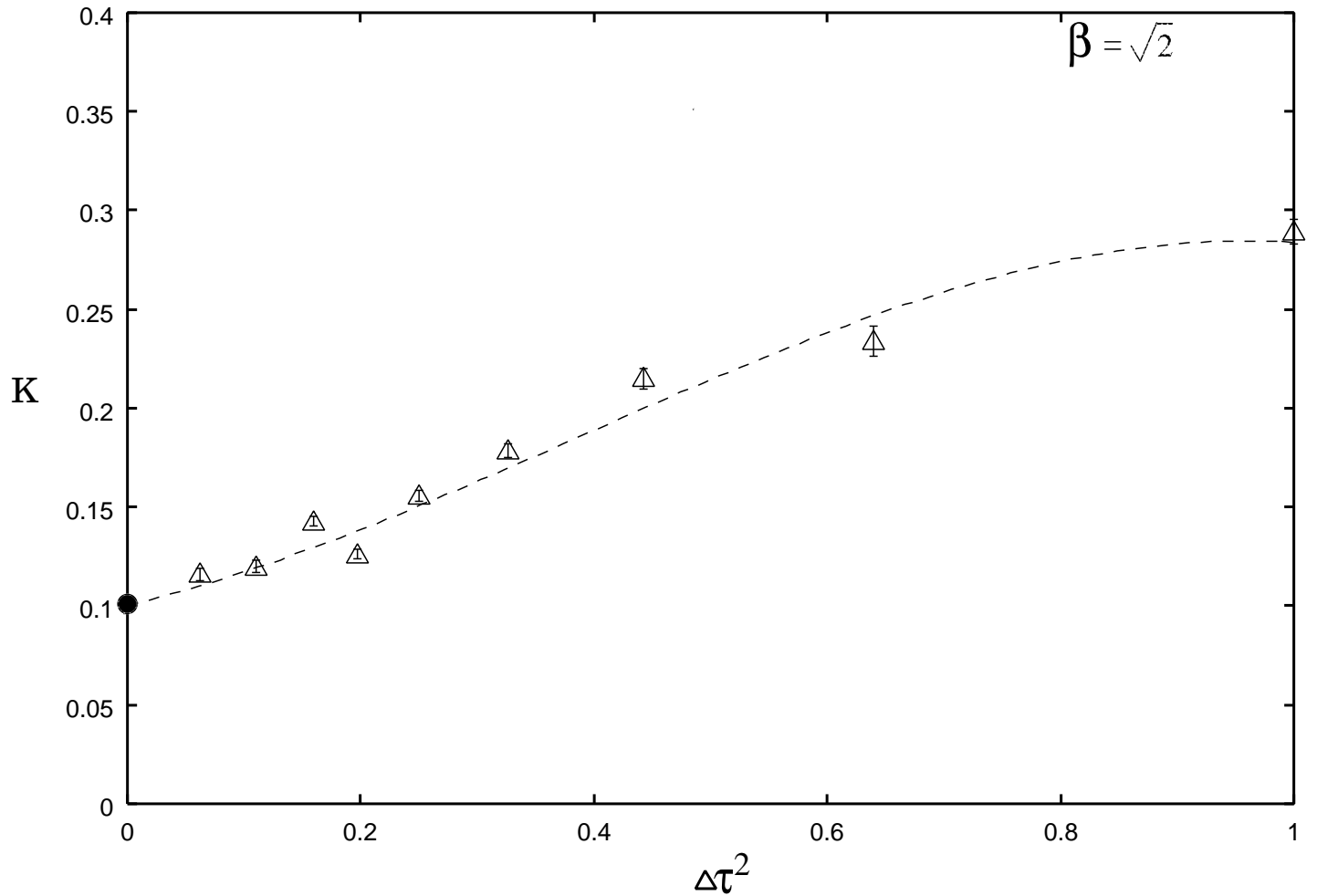


FIG. 9. String tension, K , as a function of $\Delta\tau^2$ at $\beta = \sqrt{2}$. An extrapolation to the Hamiltonian limit is performed by a cubic fit and shown by the dashed line. Our MC estimates are shown by triangles and an earlier Hamiltonian series estimate [30] is shown by a solid circle.

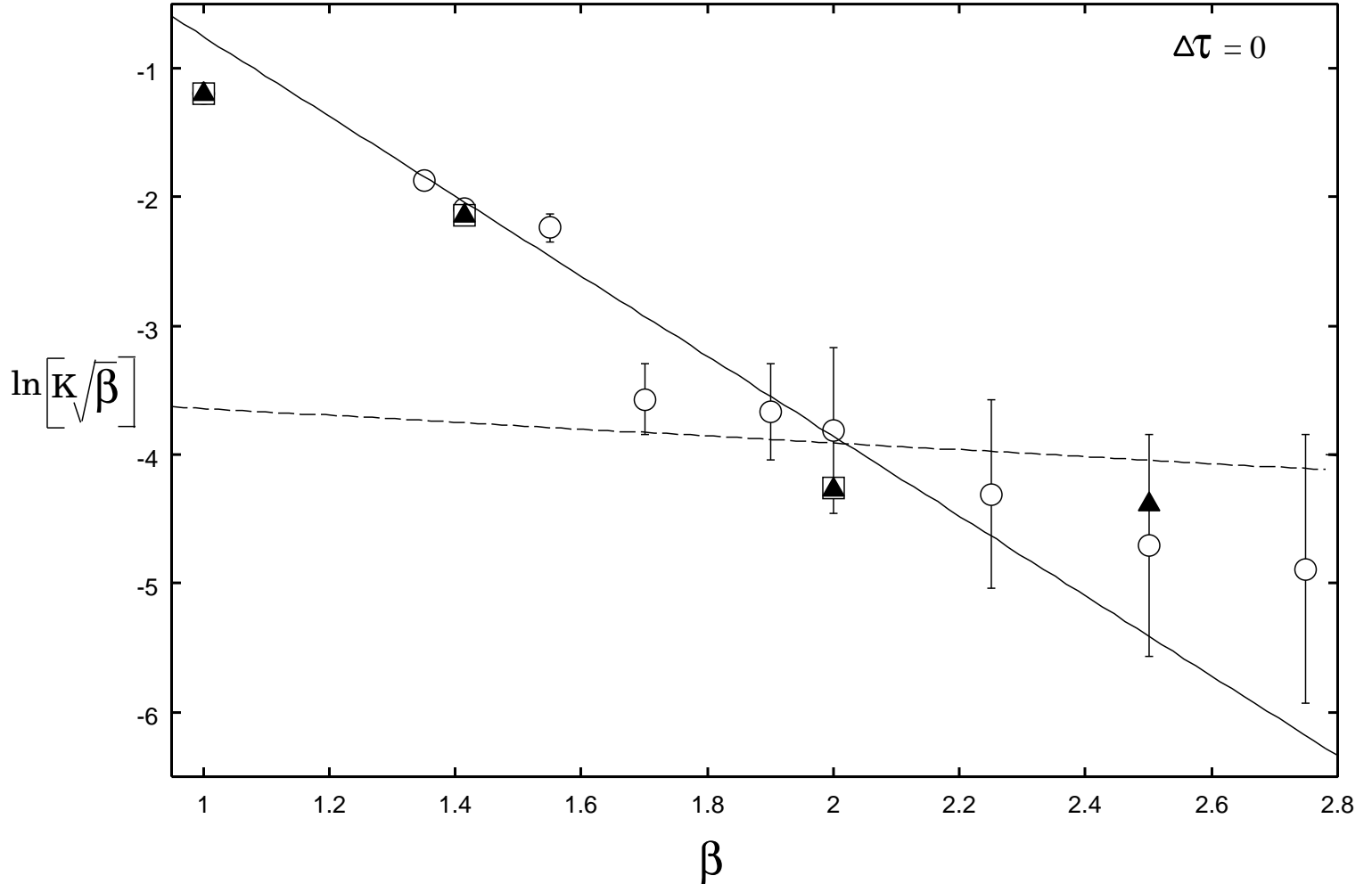


FIG. 10. Graph showing estimates of the string tension in the Hamiltonian limit as a function of β . The solid line is a least square fit to the form $K = \beta^{-1/2}\exp(a_0 - a_1\beta)$, with $a_0 = 2.359$ and $a_1 = 3.159$. The dashed line represents the finite size scaling behaviour [40]. Earlier results from an exact linked cluster expansion [50] and quantum Monte Carlo simulations [12] are shown as solid triangles and squares respectively.

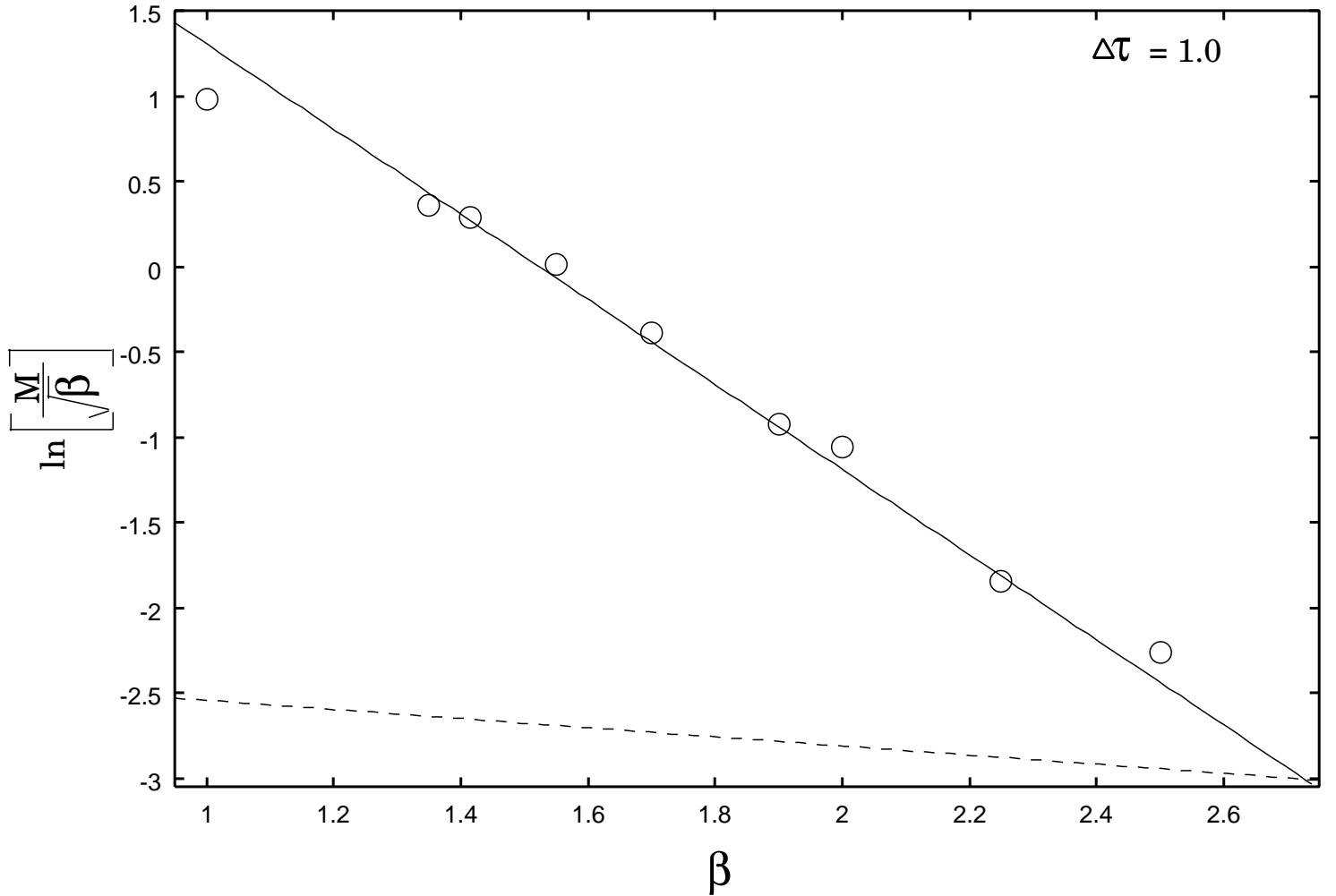


FIG. 11. The scaling behaviour of the antisymmetric mass gap against β at $\Delta\tau = 1.0$. The solid line is a fit of the form eq. (30). The errors are smaller than the symbols. The dashed line shows the finite size scaling behaviour [51]

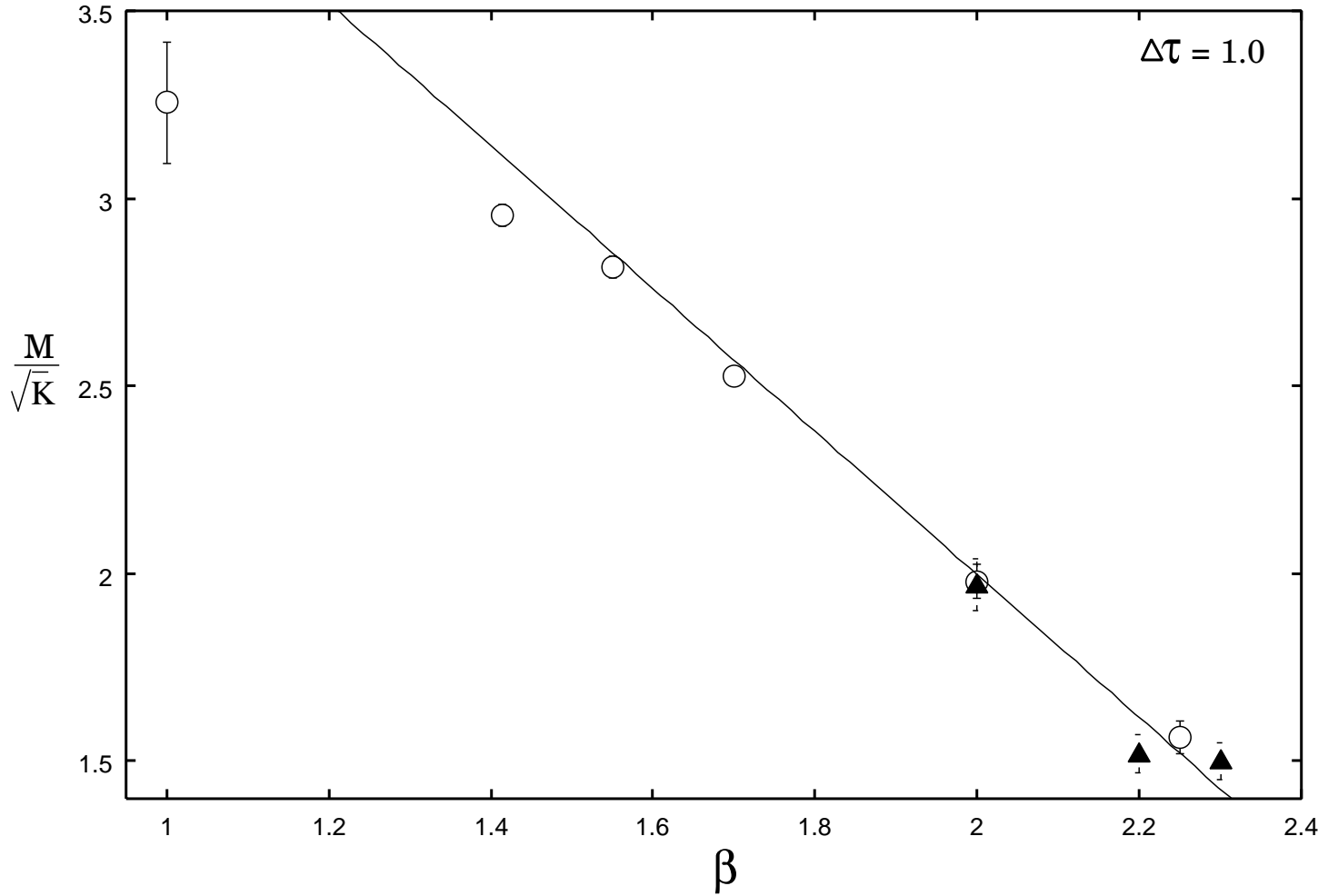


FIG. 12. The dimensionless ratio M/\sqrt{K} as a function β . Our estimates are shown by circles and solid triangles show the earlier results of Teper [47]. The solid curve represents the predicted weak-coupling behaviour.

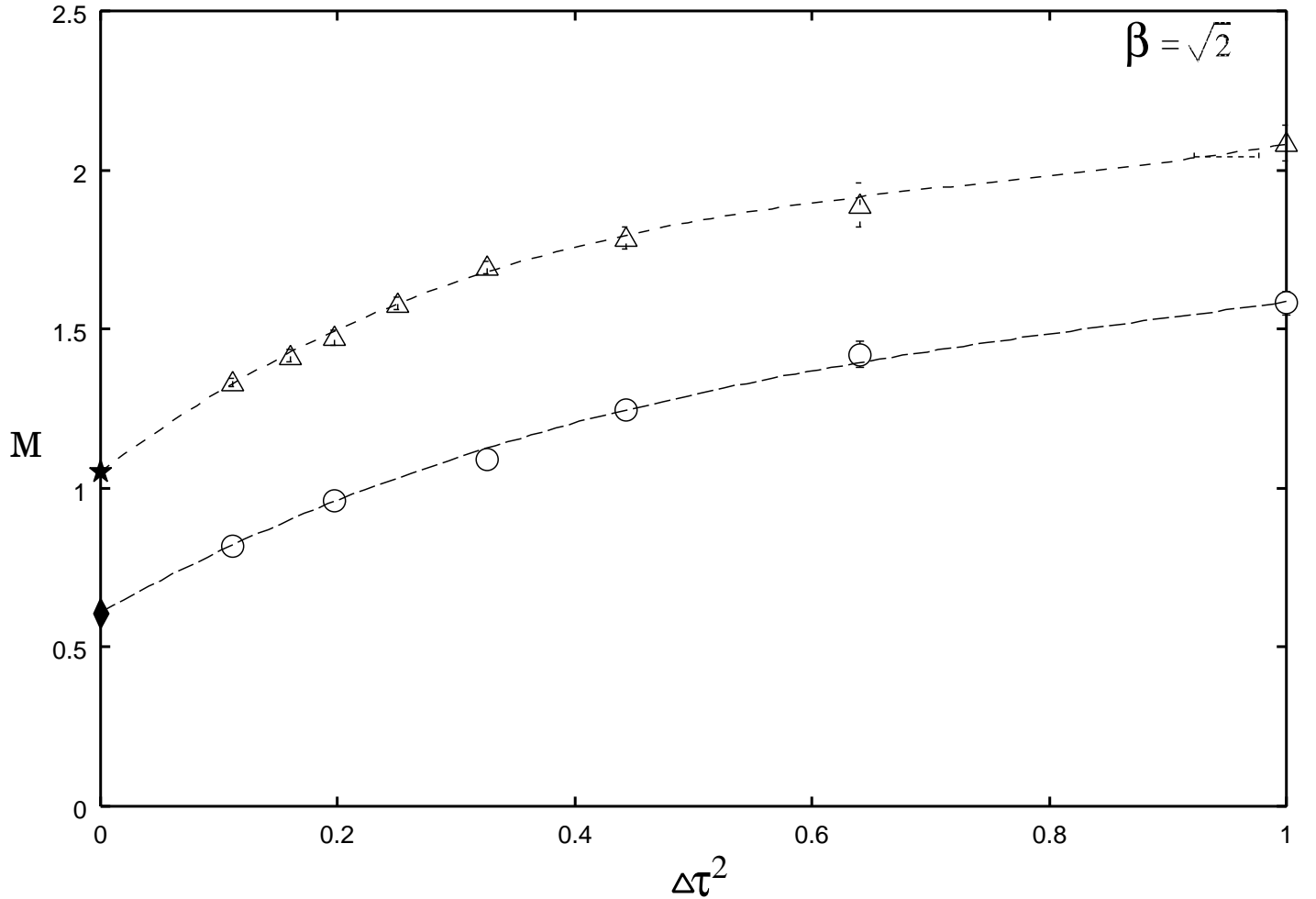


FIG. 13. Estimates of the masses of 0^{++} and 0^{--} glueballs against $\Delta\tau^2$. Results at $\beta = \sqrt{2}$ for the 0^{++} and 0^{--} are labeled by circles and triangle respectively. The solid and dashed curves are the cubic fits to the data extrapolated to the Hamiltonian limit. The series estimates of Hamer et al [30] in the limit $\Delta\tau \rightarrow 0$, for symmetric and antisymmetric channels are shown as a star and diamond respectively.

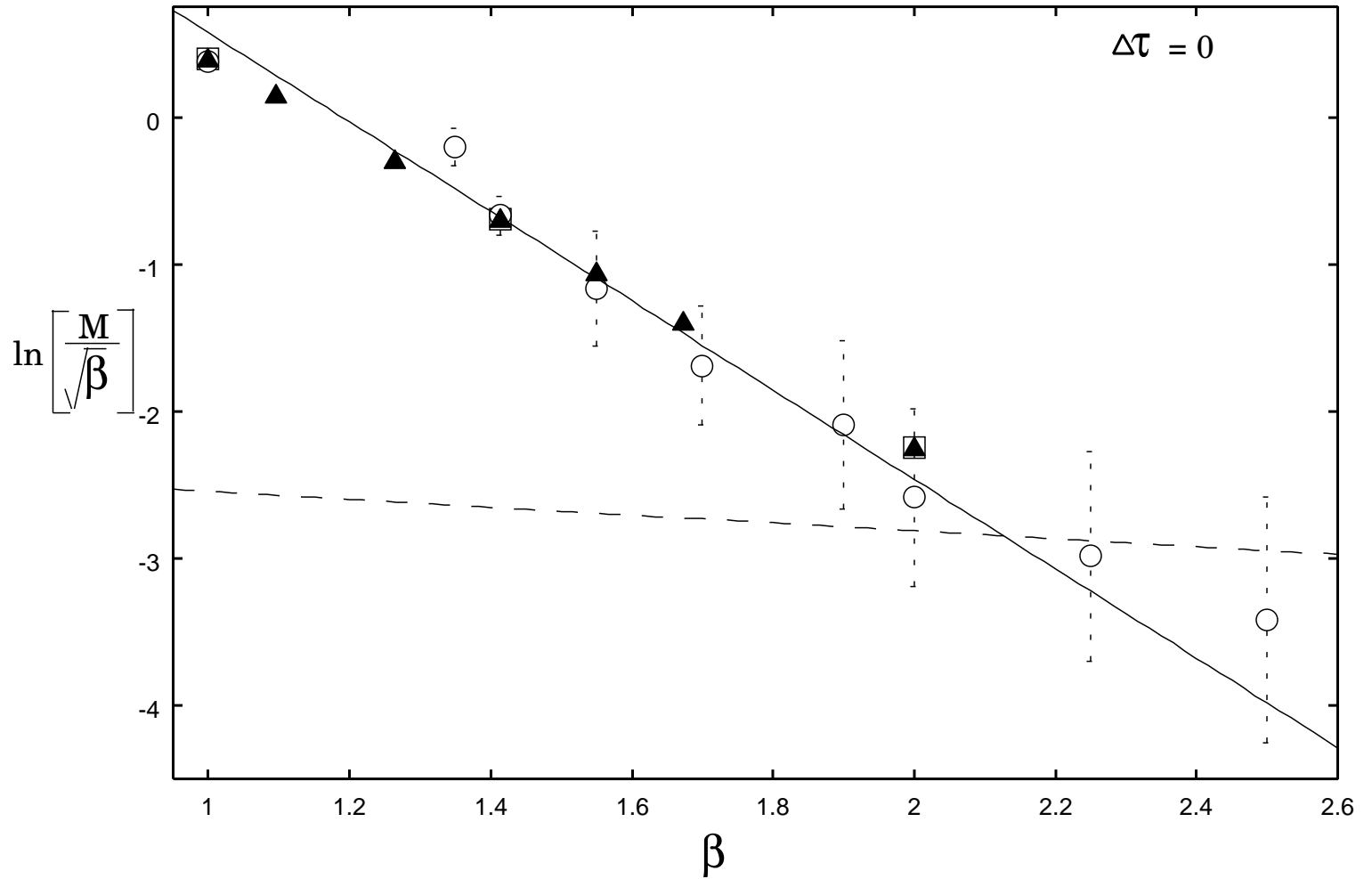


FIG. 14. Hamiltonian estimates of the antisymmetric mass gap plotted as a function of β . The solid curve is the fit to the data for $1.55 < \beta < 2.5$. The dashed line represents the finite size effects [51]. The previous results from series expansion [30] and quantum Monte Carlo calculations [12] are shown as solid triangles and open squares respectively.

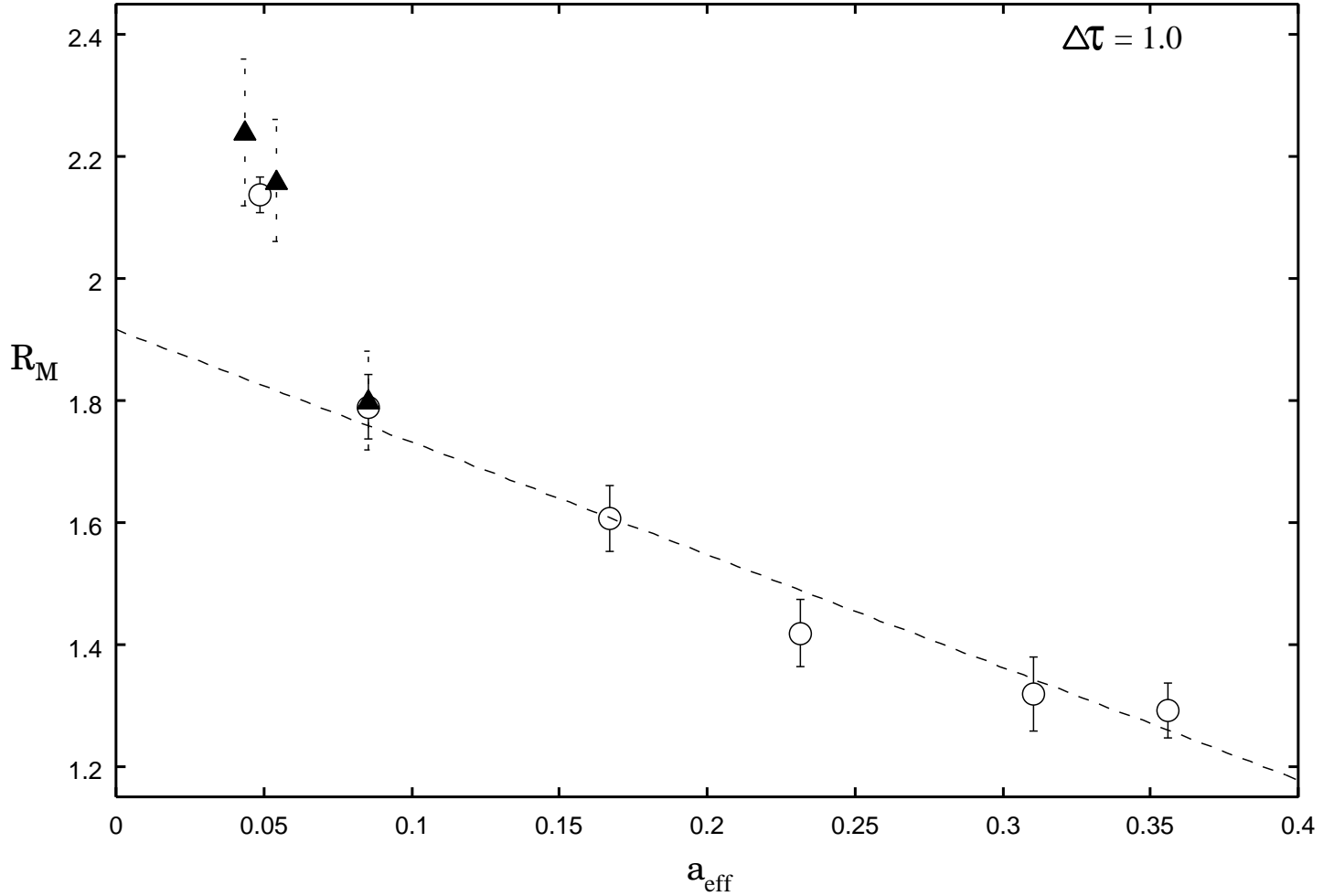


FIG. 15. A graph showing estimates of the mass ratio R_M as a function of the effective spacing, a_{eff} , at $\Delta\tau = 1.0$. Our present estimates are shown by the circles. The dashed line is a linear fit to the data over the range $0.08 \leq a_{\text{eff}} \leq 0.35$. The solid triangles show the previous estimates of Teper [47].

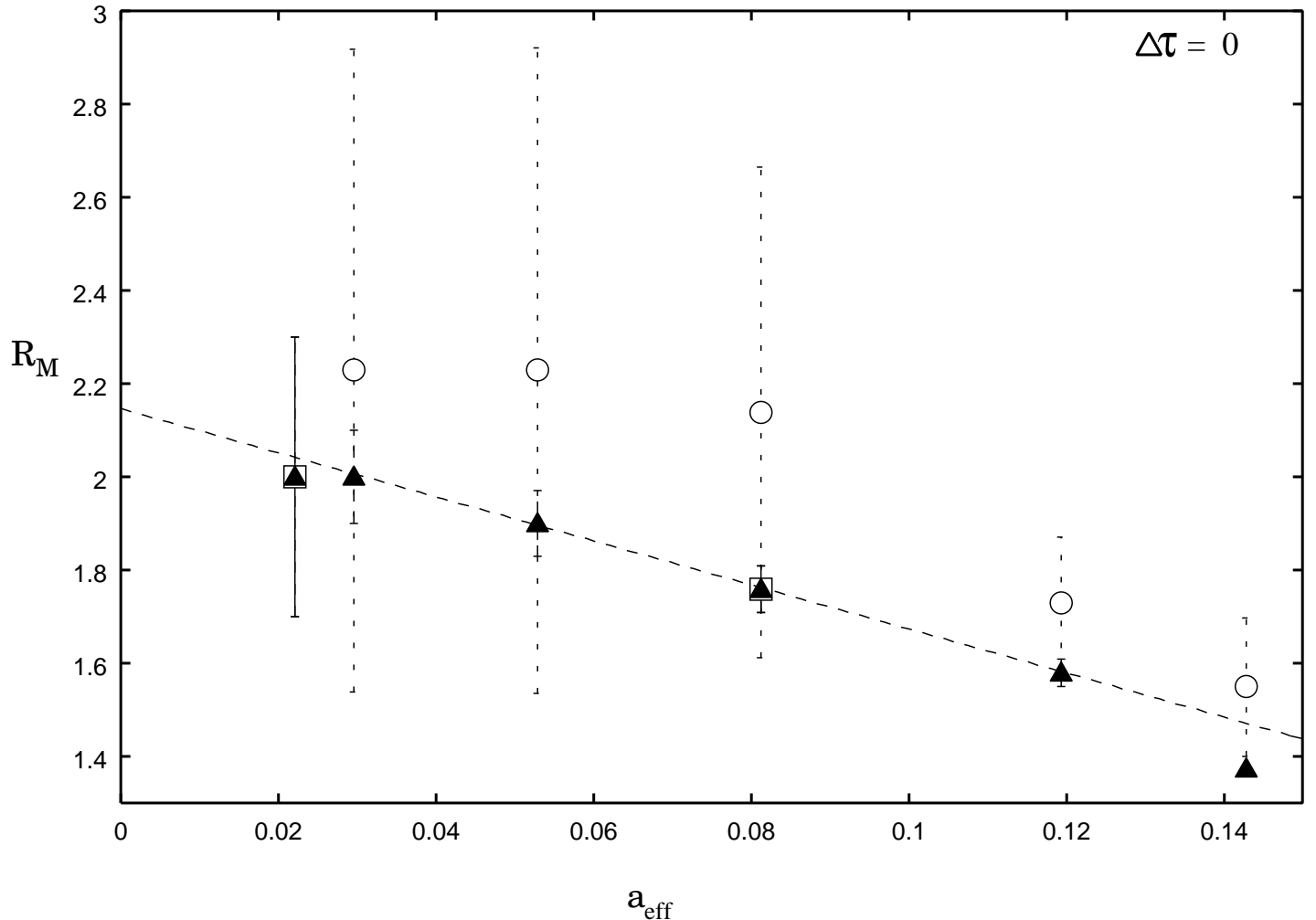


FIG. 16. Mass ratio in the Hamiltonian limit as a function of the effective spacing, a_{eff} , at $\Delta\tau = 0$. Our MC estimates are shown by the circles. Earlier series [30], and quantum Monte Carlo [20] results are shown by solid triangles and open squares respectively. The dashed line is a linear fit to the earlier data from series expansions [30] over the range $0.02 \leq a_{eff} \leq 0.12$.